Correlation of Experimental and Analytical Seismic Responses of a 1:5 Scale 3-Story Reinforced Concrete Frame

Lee, Han-Seon* Woo, Sung-Woo**

ABSTRACT

A series of dynamic and static tests were conducted to observe the actual responses of a 1:5 scale 3-story reinforced concrete(RC) frame which was designed only for gravity loads. One of the major objectives of these experiments is to provide the calibration to the available static and dynamic inelastic analysis techniques.

In this study, the experimental results were simulated by using a nonlinear analysis program for reinforced concrete frame, IDARC-2D. The evaluation of the degree of the simulation leads to the conclusion that while the global behaviors such as story drifts and shears can be in general simulated with the limited accuracy in the dynamic nonlinear analysis, it is rather easy and simple to get the fairly high level of accuracy in the prediction of global and local behaviors in the static nonlinear analysis by using IDARC-2D.

Keywords : Correlation, Experiment, Analysis, Nonlinear behavior, Reinforced Concrete

* Associate Professor, Dept. of Architectural Engineering, Korea University, Korea
** Graduate Student, Dept. of Architectural Engineering, Korea University, Korea

1. Introduction

Many differing models have been proposed to describe the structural behavior of RC structures. As classified by Negro et al. (Negro and Colombo 1998), we have in general three levels of model, namely, (1) modeling at the material level, (2) global member-type models, and (3) fiber models. In this study, we chose elements of the global type for the following reasons; (1) Global models are the models which most nonlinear analysis computer codes adopt. Therefore their calibration against the experimental results are extremely needed particularly when the structures have the nonductile or nonseismic details. (2) The parameters defining the characteristics of global models have a clear meaning for the engineer, so that it becomes possible to investigate the consequences of varying these parameters. And (3) Global models are computationally inexpensive, therefore, they are the most appropriate models to be used in parametric analyses. Once the minimum level of accuracy has been defined, the model can be used to predict the results for different intensity levels, different input motions and different structural layouts.

A series of earthquake simulation tests and thereafter a pushover test were performed on a 1:5 scale three-story RC structure (Fig. 1) designed for only gravity loads. This structure has no seismic details which are usually adopted in the seismically-active regions in the world. The structure was manufactured in 1:5 scale to accommodate the capacity of the available shaking table. The experimental setups for the earthquake simulation tests and the pushover test are shown in Photo 1.

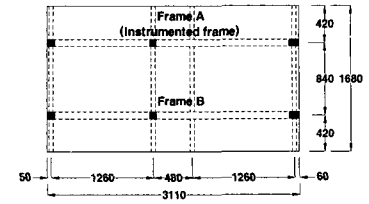

(a) Plan

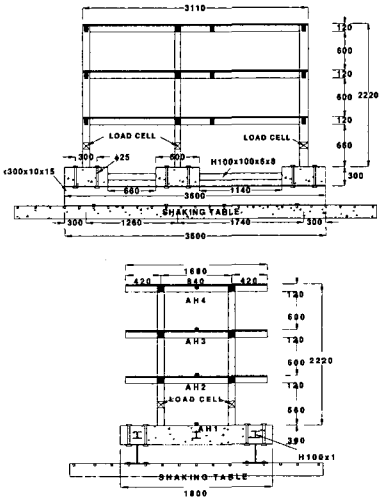

(b) Elevation

Fig. 1 1:5 scale three-story RC structure (unit: mm)

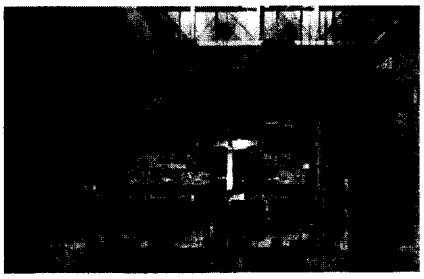

(a) Earthquake simulation test

(b) Pushover test

Photo 1 Experimental setup

The objective of these experiments and the main results are described elsewhere (Lee et al. 1998, 1999). The results of the tests were used to derive the calibrations for simple nonlinear models which will be used for the prediction of the behavior of other structural layouts used for schools, hospitals, communication centers and so on.

The computer code IDARC-2D (Valles et al. 1996), one of the codes widely used in the world for the nonlinear dynamic and static analyses of RC framed structures, was adopted. This code uses a global Takeda-like model.

The objective of this study is to find the most appropriate values of parameters in analysis by IDARC-2D to simulate the responses given by experiments and then to evaluate the degree of accuracy in the obtained simulations. Eventually, this evaluation of reliability for IDARC-2D will lead to the more careful interpretation of the results of analysis for other types of RC frame structures such as schools, hospitals, and so on.

2. Analytical Model

2.1 Material and Section Model

The material models to derive the relation between moment and curvature at the critical sections are shown in Fig. 2.

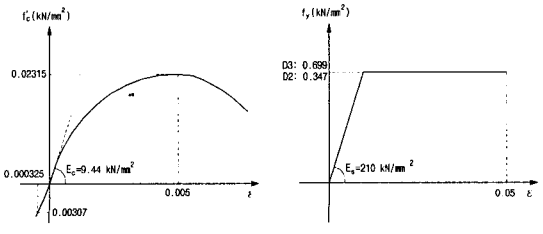

Fig. 2 Material model

The program RESPONSE developed by Mitchell and Collins (Fleber and Andreas 1990) was used to get the envelope curve for the moment-curvature relations, as depicted in Fig. 3, from the material model. The effective width (410 mm) of ACI 318-95 was used to model the relation between the curvature and the moment for the time history analyses. But the full width (840 mm) as well as the effective width (410 mm) were adopted to simulate the pushover test.

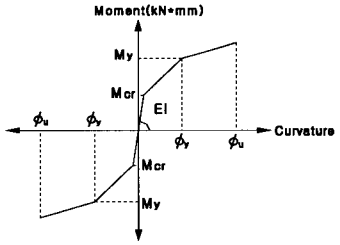

(a) Notation for Input Trilinear Envelopes for IDARC-2D

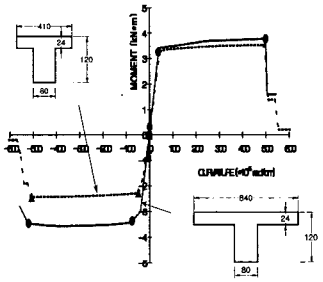

(b) Envelope curve for T beams by RESPONSE

Fig. 3 Moment-curvature envelops

2.2 M-ϕ Hysteretic Model

The three-parameter "Park hysteretic model" was first proposed by Park et al. (Park, Reinhorn and Kunnath 1987) as part of the original release of IDARC. The hysteretic model incorporates stiffness degradation, strength deterioration, non-symmetric response, slip-lock, and a trilinear monotonic envelope. The model traces the

hysteretic behavior of an element as it changes from one linear stage to another, depending on the history of deformations. The model is therefore piece-wise linear.

Each linear stage is referred to as a branch. Fig. 4 show the influence of various degrading parameters on the shape of the hysteretic loops. For a complete description of the hysteretic model see Park et al.

Fig. 4 and Table 1 provide a number of qualitative insights into modeling of the hysteretic parameters. An increase in HC retards the amount of stiffness degradation; an increase in HBD, HBE accelerates the strength deterioration; and an increase in HS reduces the amount of slip.

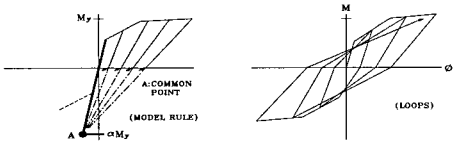

(a) Stiffness degrading parameter

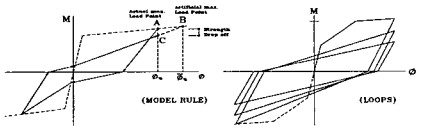

(b) Strength deterioration parameter

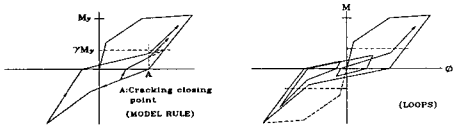

(c) Slip control parameter

Fig. 4 M- ϕ hysteretic model

Aycardi, Mander, and Reinhorn used α = 0.5, β = 0.04, and γ = 0.7 based on the experimental test results for elements (Aycardi, Mander and Reinhorn 1992). Stiffness degradation in the model is severer than the prototype, and α value between 0.5 and 1.0 has been used in the analytical model which is scaled as 1/4 or below (Reinhorn, Kunnath and Valles 1996). In this study, the hysteretic parameters are determined to simulate the test results as shown in Table 1.

Table 1 Typical range of value for hysteretic Parameters

Para-meter	Meaning	Value	Effect	Input value
α (HC)	Stiffness degrading parameter	0.1 2.0 10.0	Severe degradation Nominal degradation (default) Negligible degradation	0.5
β (HBD)	Strength degrading parameter (ductility-based)	0.0 0.1 0.4	No degradation (default) Nominal deterioration Severe deterioration	0.0
β (HBE)	Strength degrading parameter (energy -controlled)	0.0 0.1 0.4	No deterioration Nominal deterioration (default) Severe deterioration	0.04
γ (HS)	Slip or crack-closing parameter	0.1 0.5 1.0	Extremely pinched loops Nominal pinching No pinching (default)	0.7

2.3 Member Model

When the member experiences inelastic deformations, cracks tend to spread from the joint interface resulting in curvature distribution as shown in Fig. 5(a). Sections along the element will also exhibit different flexibility characteristics, depending on the degree of inelasticity observed. The program IDARC-2D includes a spread plasticity formulation and yield penetration model to capture the variation of the section flexibility and combine them to determine the element stiffness matrix. Two cases for the moment distribution are identified: single curvature and double curvature moment diagrams, and the flexibility distribution in the structural elements is assumed to follow the distribution shown in Fig. 5(b).

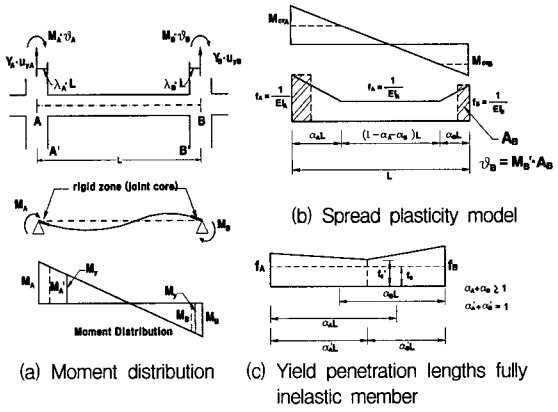

(a) Moment distribution (b) Spread plasticity model (c) Yield penetration lengths fully inelastic member

Fig. 5 Member model

2.4 Structural Model

The structural model is shown in Fig. 6. Concentrated loads on the girders represent the artificial weight loaded to compensate the mass according to the similitude load. Hence, the girders were divided into three elements which also represent properly the change in the reinforcement of the sections. The damping ratio was assumed to be 4% as found in the free vibration tests.

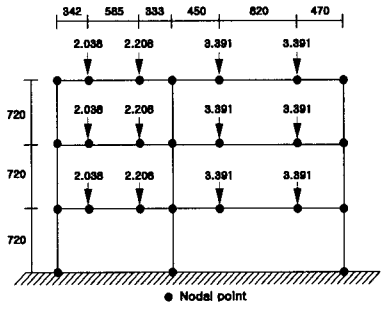

Fig. 6 Structural model (unit: mm, kN)

3. Comparison of Dynamic Behaviors

The program of tests is shown in Table 2. Before and after each earthquake simulation test, free vibration tests were performed to identify the dynamic characteristics of the model structures such as the natural period and damping ratio. The adopted input ground accelerogram is the 1952 Taft earthquake, N21E component. But the magnitude of the peak ground acceleration (PGA) was modified to 0.12g, 0.2g, 0.3g, and 0.4g. Each input motion represents the earthquake stated in the remarks of Table 2. But, Since the ultimate capacity of the structure could not be found by the capacity of the used shake table, a pushover test was performed to observe the elastic and inelastic behaviors and ultimate capacity of the sturcture after earthquake simulation test.

Instruments to record the responses, such as story displacements and accelerations, were attached to each floor and base of the model structure. Load cells were installed at the mid-height of the first story columns to measure the shear forces. Strain-gauge type displacement transducers and linear potentiometers were installed around selected exterior and interior beam-column joints to measure relative rotations near the joints.

Table 2 Test program

Test description		Remarks (Return Period)
Earthquake Simulation Test (Taft N21E)	TFT_012 (PGA 0.12g)	Design earthquake in Korea (475 years)
	TFT_02 (PGA 0.2g)	Max. earthquake in Korea (1000 years)
	TFT_03 (PGA 0.3g)	Max. considered earthquake in Korea (2000 years)
	TFT_04 (PGA 0.4g)	Severe earthquake in high seismic regions of the world
Pushover Static Test		For ultimate strength of the structure

3.1 Time History Analysis

Though the time history analyses corresponding to all the earthquake simulation tests were performed, the correlation of

experiment and analysis will be investigated only for the case of PGA 0.4g in this paper. In particular, to simulate the continuous shake-table testing, time history analysis for PGA 0.4g case was preceded by that for the case of PGA 0.3g

3.2 Fundamental Period

The fundamental period, 0.26 second, obtained through analysis appears to be similar to the test result, 0.23 second. The empirical equation given UBC 97 (ICBO 1997) gives $T = [\, C_t (h_n)^{3/4} \,] r_t = 0.197$ sec. ($C_t = 0.0731$, $h_n = 11\ m$ (for prototype), r_t (time scale factor) $= 1/\sqrt{5}$). This empirical code formulation, based on observed response of buildings in California that include the stiffening effect of nonstructural walls and cladding, may considerably overpredict the stiffness characteristics of flexible gravity load designed frames (Bracci, Reinhorn and Mander 1995).

3.3 Drift History

The parameters determining hysteretic behavior in M-ϕ relation have actually been adjusted to simulate the response, particularly, the roof drift most closely. These parameters are shown in Table 1. Though the roof drift history shown in Fig. 7 is the best

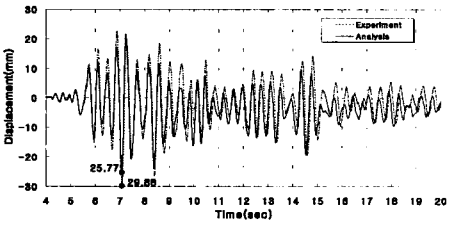

Fig. 7 Comparison of roof drift history

simulation, there is still discrepancy of 4.11 mm (about 14%) in maximum values and in phase in the latter part. The writers have tried several different sets of parameters but have found that the IDARC-2D has some numerical instability problems, and felt a difficulty with the identification of the errors because no statement was given for the reason of the termination of computer running.

The envelopes of story drifts appear to be similar in both experiment and analysis as shown Fig. 8. The largest interstory drift occurred at the second story in both of experiment and analysis. The increase in story drift was almost proportional to the excitation level, except for the second floor during 0.4g that was due to a soft-story effect resulting from higher mode participation.

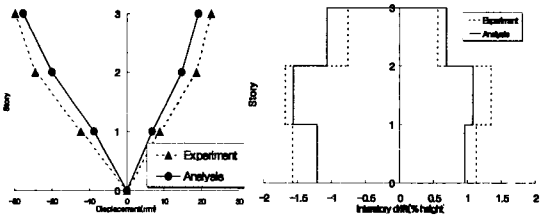

(a) Displacement profiles (b) Interstory drift envelopes

Fig. 8 Displacement profiles and interstory drift envelopes

3.4 Story Shear Versus Interstory Drift

The hysteretic curves showing the relation between the base shear and the interstory drift at the first story are shown in Fig. 9. Fig. 9(a) and (b) show the difference in the hysteretic curves for the base shear obtained by the sum of inertia forces and by the sum of column shear forces. The former case has more energy than the latter case since the inertia forces are actually the sum of damping forces and restoring column shears, though the maximum value of base shear or drift

would be approximately the same for both cases. The shape of and the energy dissipation in the hysteretic curve of analysis are quite different from those of the experiment. The discrepancy in strength is about 20%. It can be also noted that whereas the story stiffness at the first story appeared to be similar, the yielding phenomenon could not be simulated by the analysis (Fig. 9).

Fig. 10 depicts the hysteretic relation between story drift and story shear for upper stories. Story stiffnesses are very similar between analysis and experiment except the third story. However, the amount of energy dissipation and yielding phenomena could not be simulated successfully in these upper stories either. Fig. 11 compares the time histories of the absorbed energy. Total amount of absorbed energy in analysis is smaller than that in experiment by approximately 30%.

Also, the distribution of the absorbed energy over the stories from the experiment is 51% (1st story) : 43% (2nd story) : 6% (3rd story) whereas that from analysis is 43% : 40% : 17%. This implies that the analysis underestimates the trend of the concentration of energy dissipation to the lower stories.

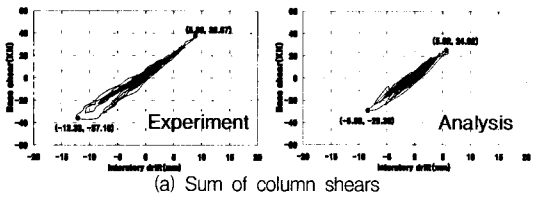

(a) Sum of column shears

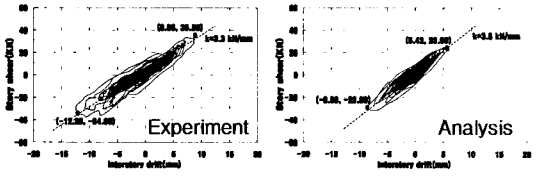

(b) Sum of inertia forces

Fig. 9 Base shear versus interstory drift at first story

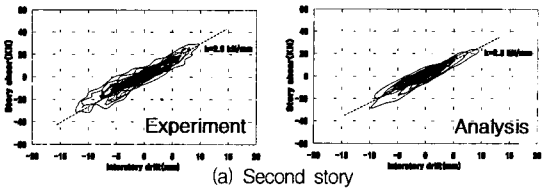

(a) Second story

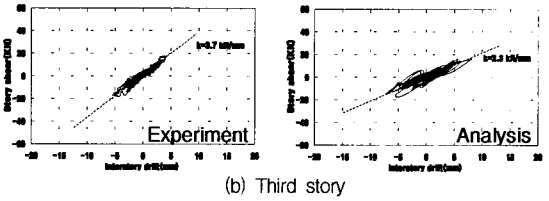

(b) Third story

Fig. 10 Interstory drift versus story shear

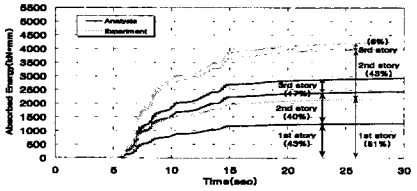

Fig. 11 Time histories of story-level absorbed energy

3.5 Story Dirft and Accelerations

Though the peak drift at the roof in analysis is smaller than in experiment as shown in Fig. 12, the peak response acceleration at the roof in analysis appears to be similar to that in experiment as shown Fig. 13. The discrepancy in the maximum base shear between analysis and experiment can be attributed to the stronger effects of the second or higher mode in analysis as shown in Fig. 13. This figure reveals that the time histories of the acceleration at the second and third floors in analysis are quite different from those in experiment and have much more predominancy in frequencies of the higher modes.

However, the histories of story drifts (Fig. 12) are similar in shape in both cases of analysis and experiment, indicating that the first mode governs, though the peak values are different.

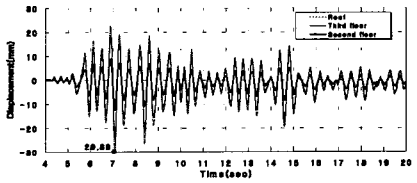

(a) Experiment

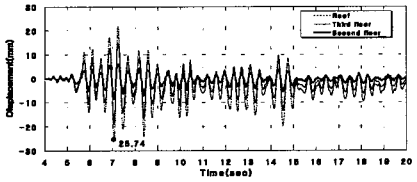

(b) Analysis

Fig. 12 Time histories of story drifts

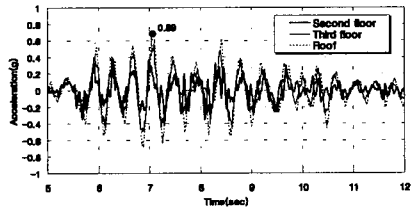

(a) Experiment

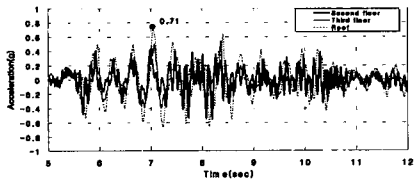

(b) Analysis

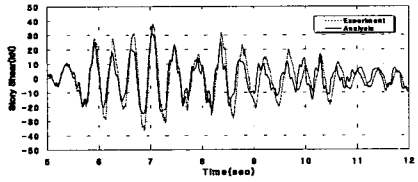

(c) Comparison of base shear derived from inertia force

Fig. 13 Comparison of story accelerations and base shear

3.6 Local Behaviors

The time histories of column shears in Fig. 14 reveals that the analysis could not simulate the bias in the shear force caused by the increase of shear stiffness due to the increase of the axial compressive forces in columns.

The angular rotations in some ends of beams and columns were measured as shown in Fig. 15. The distance over which this angle was measured is the depth of beams and the dimension of the section parallel to the shaking direction in columns. The angular rotations were calculated from the curvature at the end of members in analysis by multiplying this curvature ϕ with the length of potential plastic hinges. Fig. 16 compares the time histories of angular rotations obtained from experiment and analysis.

Generally, the magnitude of angular rotations in analysis is much smaller than that in experiment as shown in Figs. 16 and 17. The discrepancy in magnitude is considered due to the member modeling of spread plasticity in IDARC-2D.

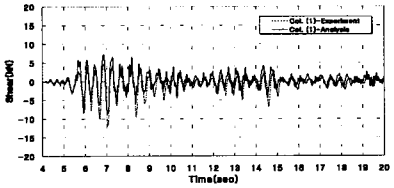

(a) Column 1

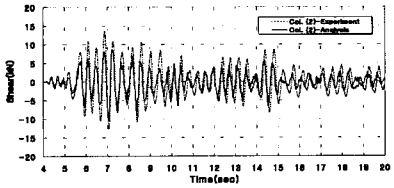

(b) Column 2

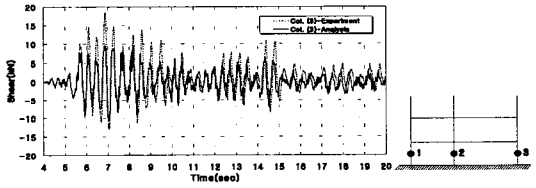

(c) Column 3

Fig. 14 Time histories of column shears at first story

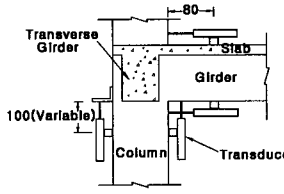

Fig. 15 Dimension and location of transducers to measure angular rotations (unit : mm)

3.7 Crack Pattern and Distributions of Plastic Hinges

The model structure did not show serious damage even after the test of Taft 0.4g test simulating the severe earthquake in the high seismic zone of the world. There was no apparent crack after Taft 0.12g and Taft 0.2g tests. After Taft 0.3g test the flexural crack can be noticed at the location (1) in Fig. 18. Several minor cracks occurred during the test of Taft 0.4g as shown in Fig. 18.

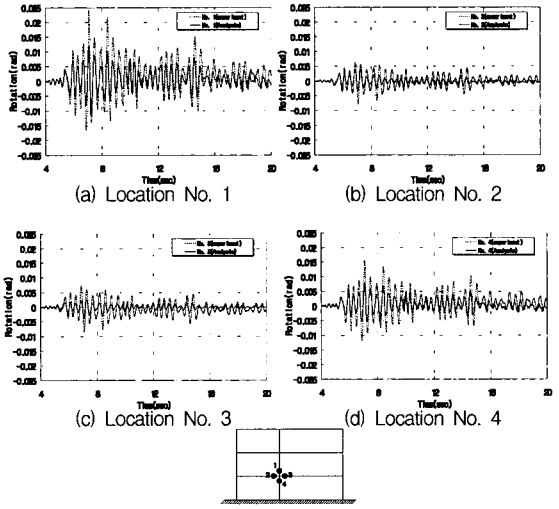

(a) Location No. 1 (b) Location No. 2

(c) Location No. 3 (d) Location No. 4

Fig. 16 Time histories of angular rotations around interior joint

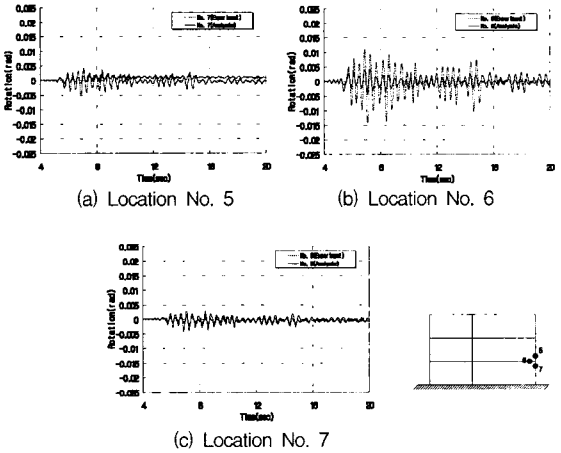

(a) Location No. 5 (b) Location No. 6

(c) Location No. 7

Fig. 17 Time histories of angular rotations around exterior joint

The beam ends at the exterior joint of the second floor have significant cracks at locations (2), (3), (4), (5), in Fig. 18, and this implies the yield at the corresponding ends of girders. In particular, the exterior columns at the first story have revealed both the flexural and shear cracks at locations (6), (7) and (8) as shown in this figure.

The analysis shows the distributions of plastic hinges in Fig. 19. The cracks shown in Fig. 18 do no appear to match the locations of plastic hinges in Fig. 19. It is interesting to note that though the interior columns at the second story have formed plastic hinges in analysis and experienced large deformations in experiment, they had actually no apparent cracks after earthquake simulation tests.

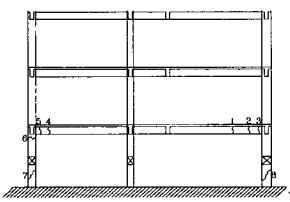

Fig. 18 Crack pattern

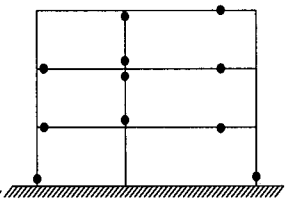

Fig. 19 Distribution of plastic hinges

4. Comparison of Static Behaviors

For earthquake simulation tests, the 1:5 model structure did not show serious damage even after Taft 0.40g test. However, due to the limitation in the capacity of the used shaking table, it was impossible to implement higher level of earthquake simulation test. Therefore, in order to get more information on the capacities (strength, deformability and so on) of the model structure, pushover test or monotonically-increasing lateral load static test was conducted. The details on the procedure and the test results are given

elsewhere (Lee et al. 1999).

The model for pushover analysis is the same as that for time history analysis except that the artificial weight to compensate the gravity weight was distributed over the slabs instead of being concentrated weights. To take into consideration the increase in the contribution of slabs at ultimate strength of structure, two sections were considered to model T beams(the effective width of T beam = 410 mm (PUSH-I), =840 mm (PUSH-II)) as shown in Fig. 3

The relations between the lateral load and the roof drift are shown in Fig. 20. The findings regarding this figure are as follows : (1) IDARC-2D could not predict or simulate the brittle failure at ultimate failure. (2) PUSH-II has indicated lower strength than that by experiment. The difference is about 8 kN (17%). (3) The additional contribution of the enlarged width of the slab to the ultimate strength is about 4 kN and this does not fully explain the reason for the discrepancy between analysis and experiment.

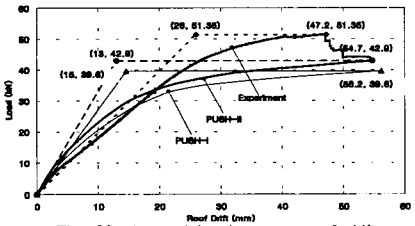

Fig. 20 Lateral load versus roof drift

4.1 Base Shear Versus Roof Drift

It can be observed from the test result in Fig. 20 that the model structure has the ultimate strength of 51.4 kN and the initial stiffness of 1.69 kN/mm. If yielding drift is assumed to be about 26 mm for the maximum drift of 47.2 mm, this model has the displacement ductility ratio of 1.57.

On the contrary, the result given by PUSH-II shows that the structure has ultimate strength of 42.9 kN and the initial stiffness of 3.33 kN/mm. When the yield displacement of 13 mm is compared to the ultimate displacement of 54.7 mm, the displacement ductility ratio in analysis turns out to be about 4. The discrepancy in the initial stiffness between analysis and experiment can be attributed to the damage implemented to the model structure during the course of earthquake simulation tests.

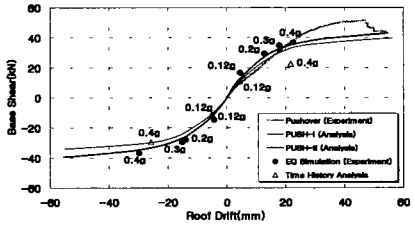

Fig. 21 Base shear versus roof drift

The points in Fig. 21 indicate the maximum base shear and the corresponding roof drift for each earthquake simulation test and are superposed on the curves of the lateral load versus the roof drift obtained from pushover test. From this figure, it can be seen that under Taft 0.20g and Taft 0.30g tests the model structure has just reached or over-reached the first significant yielding, but that Taft 0.40g test clearly implemented the yielding to the model structure. Furthermore, it is concluded that the pushover analysis can be a good tool to predict the global structural yielding phenomenon with high reliability.

4.2 Interstory drift Versus Story Shear

Fig. 22 reveals the relations between the story shear versus the interstory drift. The

ratios between interstory drifts at the failure (at ultimate strength) are very similar in experiment and analysis. The first story actually underwent the soft story mechanism. Therefore, after the ultimate strength, the first story still has an additional drift with strength drops and finally reached the compressive concrete crushing failure at the top of the interior column.

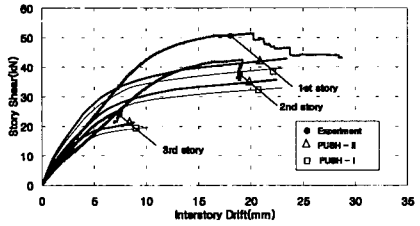

Fig. 22 Story shear versus interstory drift

The comparison of story stiffness is given in Fig. 23. The stiffness of the second story appears the smallest in the test whereas that of the third story is the smallest in the analysis. The reason for this discrepancy is also the damage implemented on the second story during the previous earthquake simulation tests.

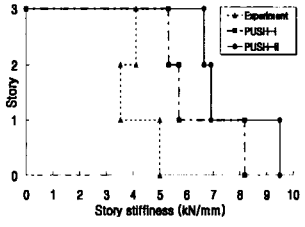

Fig. 23 Vertical distribution of initial story stiffness

4.3 Collapse Mechanism

The final distributions of plastic hinges for the two pushover analyses(PUSH-I and PUSH-II) are shown in Fig. 24(b) and 24(c) which are dissimilar from the experimental result as shown in Fig. 24(a). The collapse mechanism in experiment was the soft-story mechanism (Mechanism 1) as shown in Fig. 25(a) while those of analyses were Mechanism 2 as shown in Fig 25(b). Simple plastic analyses were performed for the two collapse mechanisms (Mechanism 1 and Mechanism 2) assuming the section properties as given PUSH-I and PUSH-II. With the section properties of PUSH-II, the two collapse mechanism have only 0.7 kN (1.8%) of difference in strength, which is almost negligible when the uncertainty in the material and section properties are considered.

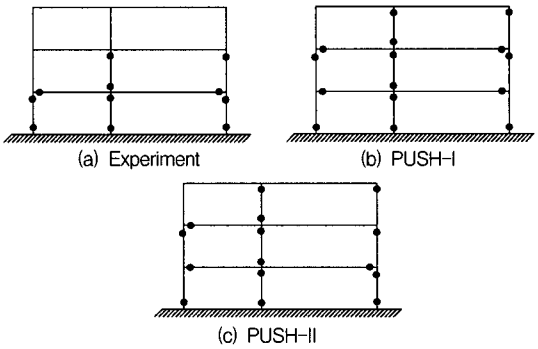

Fig. 24 Distribution of plastic hinges at the ultimate state

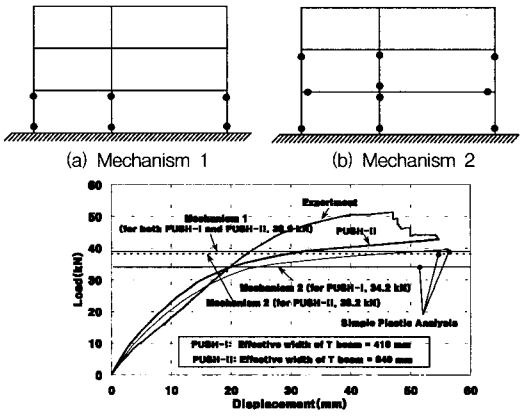

(c) Lateral load versus roof drift

Fig. 25 Collapse mechanism and collapse load

4.4 Distribution of Plastic Hinges and Damage Pattern

Fig. 26 indicates the distribution of plastic hinges and the sequence of the occurrence by

writing the magnitude of roof drift at the time of occurrence. This figure can be compared directly to the crack pattern and the sequence of crack occurrence as shown in Fig. 27. Though the occurrence of crack does not necessarily represent the yielding of the section, we can find the similarity between the distribution of cracks and that of plastic hinges. However, the sequence of the occurrence of plastic hinges appears not to correlate with that of cracks when comparing Figs. 26 and 27.

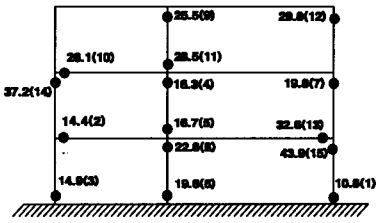

Fig. 26 Distribution of plastic hinges for PUSH-II (unit: mm)

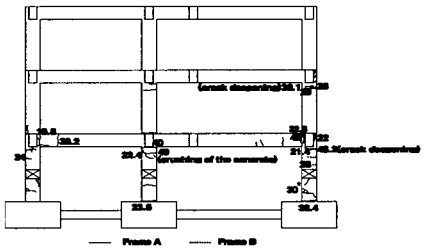

* the number denotes the roof drift when the corresponding crack occurred.

Fig. 27 Development of cracks (unit: mm)

4.5 Rotational Angles at Critical Member Ends

The rotational angles at the critical member ends were calculated in the same way as in the time history analysis. The rotational angles at the member ends at the time of the ultimate strength in experiment (roof drift = 47.2 mm) are recorded in Fig. 28 to compare with those in analysis PUSH-II.

In general, the results of experiment and analysis correlate very well. The trend of analysis is that the value obtained through analysis overestimates the angles in columns while it underestimates those in girders. However, it should be noted that the rotational angles in girders obtained by analysis are very small when compared with those given by experiment in the case of interior joint of the second floor (0.0025/0.014 and 0.0048/0.013).

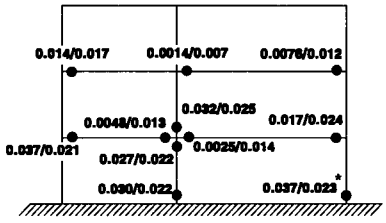

* Analysis(PUSH-II) / Experiment

Fig. 28 Comparison of rotational angles (unit : rad.)

5. Conclusions

(1) The most important question to be answered by this study is "Is the IDARC-2D capable of predicting inelastic dynamic responses of RC frames with sufficient accuracy and reliable in applying to other layouts of structures?"

The rate of success in simulating the dynamic responses given by experiment is about 75%. In other words, the damage analysis and prediction of design parameters such as story drift, story shear and maximum roof drift and so on by using IDARC-2D are not completely reliable. Thus much attention should be paid when the results of analysis are interpreted and influence the design. The followings appear to be the weak points in IDARC-2D and should be improved for

the more reliable and stable prediction of nonlinear dynamic responses of RC frames.

- The program reveals instability problems without any statement of the reason for stopping running. For example, a certain set of parameters controlling the hysteretic behavior do not get any output while other sets do.
- The global responses such as story drift and story shears as given by experimental results could not be simulated successfully even though the best efforts were devoted by the writers. This clearly suggests that there need to be more parameters to describe the hysteretic behavior or that the modeling options offered by IDARC-2D are not sufficient to describe the actual responses.
- The performance-based design concept and evaluation of the existing structure (ATC 40, FEMA 273, 274) generally require the estimation of the demand and the supply in the deformation capacity at the critical regions of the structure. Since IDARC-2D uses spread-plasticity model in member level, it is relatively inconvenient to get these values directly from the output. The method used in this study to estimate this value($\phi_{END} \times h$(hinge length)) seems to be too rough and therefore can not simulate the test result sufficiently.
- IDARC-2D could not predict or simulate the brittle failures which actually occurred in the model structure. It is the hope of the writers that, in the near future, new version of IDARC-2D or other computer codes can simulate this kind of behaviors.

(2) The comparison of the results of dynamic and static nonlinear analyses with reference to those of experiment leads to the following finding: dynamic nonlinear analysis does not necessarily provide higher level of accuracy or reliability than static nonlinear analysis as expected commonly. If the maximum values of responses such as roof drift under given design earthquake could be estimated reliably, by capacity spectrum method (ATC 40) for example, the nonlinear static analysis by IDARC-2D can provide the information on the supply and demand in forces and deformations at critical regions of structure with fairly high level of reliability.

Acknowledgement

The experiment part stated herein was supported by the Ministry of Construction and Transportation, the Republic of Korea, and several private companies including SSangYong Engineering and Construction Corp., DongBu Corp., Hyundai Construction Corp., and DongYang Structural Safety Consultants Corp. The analysis part was supported partially by the STRESS at Hanyang University which is in turn supported by Korea Science and Engineering Foundation(KOSEF). These supports are gratefully acknowledged by the writers.

References

1. Lee, H. S., Woo, S. W., "Earthquake Simulation Tests of A 1:5 Scale Gravity Load Designed 3-Story Reinforced Concrete Frame," *Journal of the Korea Concrete institute*, Vol. 10, No. 6, December 1998, pp. 241-252.
2. Lee, H. S., Woo, S. W., Heo, Y. S., and Song, J. G., "Pushover Tests of 1:5 Scale 3-Story Reinforced Concrete Frames,"

Journal of the Korea Concrete institute, Vol. 11, No. 3, July 1999, pp. 165-174.
3. Negro, P., and Colombo, A., "How Reliable Are Global Computer Models? Correlation with Large-Scale Tests", *Earthquake Spectra*, V. 14, No. 3, August 1998.
4. Valles, R.E., Reinhorn, A.M., Kunnath, S.K., Li, C., and Madan A., "IDARC 2D Version 4.0: A Program for the Inelastic Damage Analysis of Buildings", Technical Report NCEER-96-0010, State University of New York at Buffalo, 1996.
5. Felber, Andreas J., "RESPONSE: A Program to Determine the Load-Deformation Response of Reinforced Concrete Sections", M.A.Sc. thesis, Department of Civil Engineering, University of Toronto, 1990, 148 pp.
6. Park, Y.J., Reinhorn, A.M., and Kunnath, S.K., "IDARC: Inelastic Damage Analysis of Reinforced Concrete Frame-Shear-Wall Structures", Technical Report NCEER-87-0008, State University of New York at Buffalo, 1987.
7. Aycardi, L.E., Mander, J.B., and Reinhorn, A.M., "Seismic Resistance of Reinforced Concrete Frame Structures Designed Only for Gravity Loads: Part II-Experimental Performance of Subassemblages," Technical Report NCEER-92-0028, SUNY at Buffalo, 1992.
8. Reinhorn, A.M., Kunnath, S.K., and Valles, R.E., "IDARC 2D Version 4.0: A Program for the Inelastic Damage Analysis of Building," Users Manual, 1996.
9. ICBO, "Uniform Building Code," International Conference of Building Officials, Whittier, California, 1997.
10. Bracci, J.M., Reinhorn, A.M., and Mander, J.B., "Seismic Resistance of Reinforced Concrete Frame Structures Designed for Gravity Loads: Performance of Structural System," ACI Structural Journal, V. 92, No. 5, September-October 1995, pp. 597-609.
11. ATC, "Seismic evaluation and retrofit of concrete building: Volume 1, 2," ATC-40 Report, Applied Technology Council, Redwood City, California, 1996.
12. BSSC, "NEHRP Guidelines for the Seismic Rehabilitation of Buildings," ATC-33 project, BSSC, FEMA 273, 1996.
13. BSSC, "NEHRP Commentary on the Guidelines for the Seismic Rehabilitation of Buildings," ATC-33 project, BSSC, FEMA 274, 1996.